Molecular Catalysis xxx (xxxx) xxx–xxx

Contents lists available at ScienceDirect

Molecular Catalysis

journal homepage: www.elsevier.com/locate/mcat

# Thermo-chemically tuning of active basic sites on nanoarchitectured silica for biodiesel production

Edgar M. Sánchez Faba[a], Gabriel O. Ferrero[a], Joana M. Dias[b], Griselda A. Eimer[a,*]

[a] CITeQ-UTN-CONICET, Universidad Tecnológica Nacional, Facultad Regional Córdoba, Maestro López esq. Cruz Roja Argentina, Ciudad Universitaria, 5016, Córdoba, Argentina

[b] Departamento de Engenharia Metalúrgica e de Materiais, LEPABE, Faculdade de Engenharia, Universidade do Porto, R. Dr. Roberto Frias, 4200-465, Porto, Portugal

ARTICLE INFO

*Keywords:*
Mesoporous silica
Biodiesel
Sunflower oil
Sodium
Calcination rate

ABSTRACT

In the design of catalysts, an extremely important point is to determine, control and increase the availability of active sites on the surface. In the present work, active sodium oxide species have been identified and it is demonstrated how its dispersion can be suitably improved by combining sodium loading degree and calcination heating rate in order to increase the catalyst basic character and consequently, its performance. The different synthesized materials were characterized by: small-angle X-ray scattering (SAXS), high angle X-ray diffractions (XRD), atomic absorption spectroscopy (AA), BET method (specific surface determination), Fourier-transform infrared spectroscopy (FT-IR), carbon dioxide temperature programed desorption ($CO_2$ TPD) and X-ray photoelectron spectroscopy (XPS). The obtained catalyst using 10 wt% of sodium loading followed by calcination at 500 °C, employing an 8 °C/min heating rate, showed the highest activity towards the transesterification of sunflower oil reaction (5 h, 60 °C, 14:1 methanol to oil molar ratio, 2 wt% catalyst, vigorous magnetic stirring), achieving a 90% biodiesel yield.

## 1. Introduction

Due to the availability and low cost of petroleumdiesel fuel, biofuels obtained from vegetables oils did not get a special interest in the twenties and before. This might be caused by diesel engine design, which was not able to run with vegetable oils because of their high viscosity compared to petroleum diesel fuel [1]. However, the use of vegetable oils in diesel fuel engines resurged in times of high oil prices and shortages in the reserves, such as World War II and the oil crises of the 1970's. For this purpose, the alternative was to transform vegetable oils into fatty acid alkyl esters (Biodiesel) using a transesterification reaction. In this way, triglycerides present in vegetable oils are converted into smaller molecules, less viscous and easy to burn in a diesel engine. This process allows therefore to replace the petroleum diesel fuel by this renewable fuel.

Nowadays, the interest is still focused on biodiesel production as an alternative to replace or complement non-renewable fossil fuels, but also to help countries to reduce their dependence on imported petroleum derivatives [2]. This arises as a result of the increase in the energy demand as a result of the constant growth of the world population and the need to maintain the current life standards.

From the environmental point of view, biodiesel is an excellent option to replace conventional petroleum diesel, since it can be obtained from renewable raw materials, as vegetable oils or animal fats (the tendency is to increase the use of waste materials due to their low cost and environmental impacts). In the same way, the production of a clean biofuel is an attractive alternative for pollution mitigation [3].

The transesterification reaction can be catalyzed using either an acid or an alkali catalyst. Nevertheless, the reaction rate for alkali catalysis is faster taking into account the reaction mechanism involved, and it is possible to work at lower temperatures, compared to the acid catalyzed process [4–6].

Today, the conventional process used to produce biodiesel in the industry employs alkali hydroxides or methoxides (e.g. NaOH, $NaOCH_3$) as catalysts [7,8]. This homogenous based process in batch results in a short reaction time [9]. Nevertheless, it is extremely sensitive to the presence of water and free fatty acids (their concentration must be very low to avoid the formation of soaps as a side product, by saponification reactions) [10]. The purification of the product requires several stages, including neutralization, washing and drying, with consumption of water, energy, and the need to treat the resulting wastewater. Moreover, the catalyst cannot be reused and the by-product (glycerol) also needs to be extensively purified [11], resulting in environmental and economic disadvantages [12,13].

* Corresponding author.
*E-mail address:* geimer@frc.utn.edu.ar (G.A. Eimer).

https://doi.org/10.1016/j.mcat.2018.08.013
Received 13 June 2018; Received in revised form 9 August 2018; Accepted 19 August 2018

Some of these proposed processes achieve conversions and yields greater than 90% [14,15]. However, many of them utilize high catalyst concentration, and even high temperatures and pressures, near critical and supercritical conditions [16], non-viable for industrial application.

For such reasons, new routes are being sought for biodiesel production, and the tendency is to use heterogeneous catalysis to maximize yields and simplify the purification steps of the final product [17–19]. Solid catalysts are considered a green technology, showing the possibility of recycling and designing a continuous process. This is why the synthesis of efficient, commercially attractive and robust catalysts has become progressively challenging.

Several materials have been informed as solid catalysts, both acid and basic, for the mentioned reaction. The alkali and alkaline earth metal oxides are very studied for this purpose owing to their basic properties [7,20–22]. These oxides can be supported on porous materials to increase the exposed surface and consequently their activity, acting as Lewis bases [4]. Furthermore, taking into account the hydrophilic nature of many porous supports, these can also be modified with other species to increase the hydrophobicity, as reported by Osman et al. [23]. This mitigates problems related to the presence of water in the reaction mixture, which might lead to catalyst deactivation and, consequent, loss of the activity.

Many publications have studied the mechanism of the oil transesterification reaction and its kinetic modeling. Verhé et al. [4] described the heterogeneous mechanism (solid/liquid interaction) whereby the methanol molecule forms a methoxide when adsorbed on the solid surface where the oxide is deposited. And then, this methoxide reacts with the triglycerides present in the liquid phase.

SBA-15 mesoporous material is one of the most popular supports used to prepare solid catalysts because it can be tailored to reach unique textural properties: its highly ordered structure and hydrothermal stability (related to the thick wall), its large surface, volume and pore size distribution, make it ideal for the dispersion of metals as active centers [24]. As a result, a high mass transfer is allowed [22,25] and new properties are conferred to this material. Likewise, it is possible to discriminate molecules according to their size and to allow the diffusion of certain reagents and products [26–28], increasing the selectivity.

In this work, two important variables were investigated to obtain an efficient alkali solid catalysts for biodiesel production: the degree of metal loading and the calcination heating rate. The metal loading is important because it provides the active sites for the transesterification reaction [21,29]. The variation of calcination heating rate can also impact on the formed active species, the catalyst activation time and the consumed energy in this process.

Combining these two factors and in order to reach the highest conversion in an adequate time at moderate reaction conditions, a series of Na/SBA-15 catalysts was synthesized with different sodium loadings (3, 5, 10 and 15 wt%) and considering different calcination heating rates (2, 5, 8 and 15 °C/min). The activity of the prepared catalysts was evaluated in the transesterification of sunflower oil.

## 2. Experimental

### 2.1. Materials

Sunflower oil was purchased in a local market. Tetraethyl orthosilicate (TEOS) and triblock copolymer Pluronic 123 were provided by Sigma-Aldrich. Absolute methanol and isopropyl alcohol for HPLC application, were purchased from Sintorgan Reactivos. n-Hexane for liquid chromatography and hydrochloric acid were purchased from LiChrosolv Merk and Biopack, respectively. Sodium carbonate pro-analysis, hydrofluoric and nitric acids were provided by Cicarelli.

### 2.2. Catalyst preparation

SBA-15 was synthesized according to the method described by Zaho et al. [27,30]. In a typical synthesis, 4 g of triblock copolymer Pluronic 123 were mixed with 30 g of distilled water and 120 g of 2 M HCl solution, at 40 °C. When Pluronic 123 was completely dissolved, 8.5 g of TEOS were added to the mixture, and stirred for 20 h at 40 °C. The obtained suspension was kept under static condition, at 80 °C for 24 h. The solid was after filtered, washed with distilled water until neutral pH, and dried at 60 °C overnight. The powder was finally calcined at 500 °C for 8 h, using a heating rate of 1 °C/min.

The mesoporous material was modified with sodium by the wet impregnation method. The theoretical metal loadings were 3, 5, 10 and 15 wt%, referred to the catalyst mass. Sodium carbonate was chosen as the metal precursor. The calculated amount of salt was dissolved in 37.5 mL of distilled water and 0.75 g of the support were added. The suspension was stirred for 15 min and then, the solvent was evaporated in a rotary evaporator. The material was dried at 60 °C overnight, followed by calcination at 500 °C, using the heating rates of 2, 5, 8 and 15 °C/min.

The resulting catalysts were designated as Na/SBA-15 (X) RY, where X represents the theoretical sodium loading (in mass percentage) and Y represents the calcination heating rate [°C/min].

### 2.3. Catalyst characterization

Small-angle X-ray scattering patterns were recorded at ambient temperature on a Xenocs Xeuss 1.0 equipment, with a Pilatus 100 K detector and CuK$\alpha$ radiation ($\lambda$ = 0.154 nm). Data were recorded in 2$\theta$ range between 0.6° and 8°. High angle X-ray diffractions (XRD) analysis were performed in a PANalytical X-Pert Pro X-ray powder diffractometer, with a Bragg-Brentano geometry. A CuK$\alpha$ lamp was used (40 kV, 40 mA), in a 2$\theta$ range between 20° and 80°.

BET method was employed to measure the specific surface of the materials using a Micrometrics Pulse ChemiSorb 2700 equipment.

The catalysts sodium contents were determined by atomic absorption spectroscopy (AA), employing a Shimadzu AA-7000 equipment. Each catalyst was dissolved with 0.5 mL of nitric acid and 0.5 mL of hydrofluoric acid (both concentrated), and heated until a small drop was obtained. Then, this drop was diluted up to 50 mL with deionized water for further analysis.

FT-IR analysis were performed on a Thermo Scientific Nicolet iS10 spectrometer, with Smart OMNI-Transmission accessory. The measure range was from 400 to 4000 $cm^{-1}$ with a resolution of 8 $cm^{-1}$ and 50 scans. Samples were prepared by the KBr technique.

The basicity of the synthetized catalysts was studied by temperature programed desorption of carbon dioxide ($CO_2$ TPD), in a ChemiSorb 2720 equipment. Carbon dioxide is used as probe molecule due to its Lewis acidity. The analysis tube was filled with 0.04 g of the sample, and treated at 150 °C for 30 min in nitrogen atmosphere (20 mL/min). Then, temperature was set in 100 °C, and $CO_2$ (50 mL/min) was introduced for one hour. After purging with He (20 mL/min) for 45 min at 100 °C to remove $CO_2$ in the gas phase, the sample was heated up to 950 °C using a ramp of 10 °C/min, and the desorbed $CO_2$ was measured with a conductivity detector.

The XPS analysis was performed on a SPECS Multi-technique equipment, equipped with a dual X-ray source (Mg/Al) and a hemispherical analyzer PHOIBOS 150 in fixed analyzer transmission mode (FAT). The spectra were obtained with a 30 eV step energy, with Al and Mg anode operated at 200 W. The pressure during the measurement was less than 1.10–9 mbar. The samples were pressed, supported on the instrument sample holders, subjected to vacuum (10-2 mbar) for 10 min at 200 °C. Subsequently, ultra-high vacuum was applied for at least two hours before analyzing.

### 2.4. Transesterification reactions

The reactions were carried in a batch reactor, consisting of a flat bottom three neck flask, which was connected to a reflux condenser to

avoid the methanol loss and ensure reflux.

The chosen reaction conditions were: methanol to oil molar ratio 14:1, 2 wt% catalyst concentration (referred to the oil mass), temperature of 60 °C, and vigorous magnetic stirring. All the essays were carried out for 5 h.

In the beginning, the catalyst was mixed with the appropriate methanol mass for 10 min, at ambient temperature. After this, 5 mL of oil were added to the mixture, and stirred for another 10 min. Finally, the remaining oil mass was added, and the reactor was taken to the bath at 60 °C.

After 5 h, the catalyst was separated by filtration and the methanol excess was recovered from the reaction products in a rotary evaporator. To ensure separation of biodiesel and glycerol, products were settled in a separatory funnel overnight. Then, biodiesel was kept in a freezer until its analysis.

All reactions were performed at least in duplicate. The results were expressed as mean values, with relative percentage differences between them always < 5% of the mean.

### 2.5. Methyl ester quantification

Samples were analyzed by high performance liquid chromatography following the method described by Carvalho et al. [31]. A Perkin Elmer Series 200 HPLC was used, equipped with a UV/visible detector, a Vertex Plus (250 mm × 4.6 mm, 5 µm) Eurospher II 100-5 C18 P column, and a 20 µl injection loop.

Samples preparation was made diluting 10 µL of each reaction mixture in 4 mL of isopropyl alcohol. The diluted samples were filtered with a 0.45 µm syringe filter before being injected.

FAME yield was then calculated taking into account the integrated areas of the obtained chromatograms [31].

## 3. Results and discussion

Table 1 exposes the sodium content and the specific surface of all the synthetized catalysts (calcined at different heating rates), together with the obtained FAME yields when they were probed in the transesterification reaction of sunflower oil with absolute methanol.

For a given heating rate (e.g. 8 °C/min), the SBA-15 specific surface decreases according with the Na loading increment, possibly due to a loss of structural regularity (Table 1) and filling or blocking of some mesopores by the sodium species present [33].

**Table 1**
Chemical composition and structural properties of the synthetized catalysts, together with the obtained FAME yields.

| Material | Na content[a] [wt %] | Calcination heating rate [°C/min] | Specific area[b] [$m^2$/g] | FAME Yield [%] |
|---|---|---|---|---|
| SBA-15 | – | – | 811 | – |
| Na/SBA-15 (3) | 3.2 | 2 | 209 | 20.34 |
| | | 5 | 279 | 33.04 |
| | | 8 | 314 | 56.98 |
| | | 15 | 205 | 67.99 |
| Na/SBA-15 (5) | 4.4 | 2 | 141 | 39.25 |
| | | 5 | 247 | 53.38 |
| | | 8 | 271 | 80.02 |
| | | 15 | 97 | 82.72 |
| Na/SBA-15 (10) | 10.3 | 2 | 109 | 38.57 |
| | | 5 | 207 | 60.04 |
| | | 8 | 261 | 90.04 |
| | | 15 | 52 | 93.83 |
| Na/SBA-15 (15) | 12.4 | 2 | 48 | 38.59 |
| | | 5 | 189 | 60.11 |
| | | 8 | 207 | 90.99 |
| | | 15 | 37 | 95.81 |

[a] Measured by atomic absorption spectroscopy (AA).
[b] Determined by BET method.

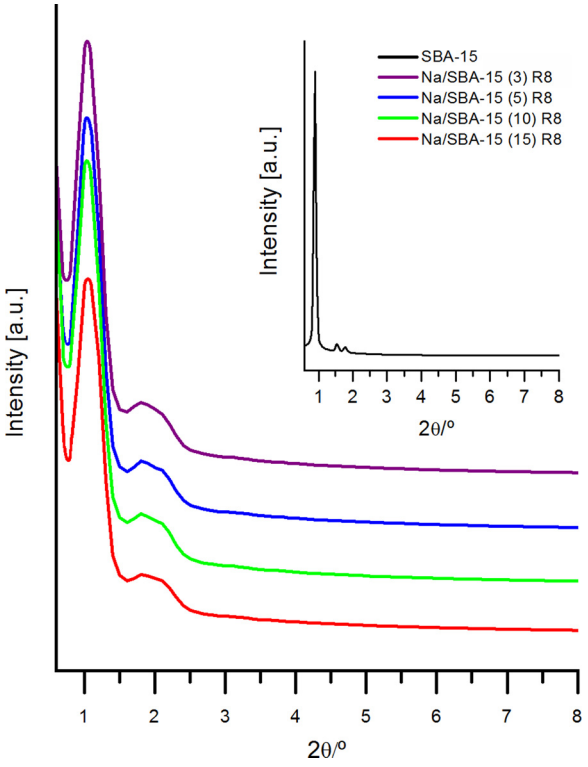


**Fig. 1.** Small-angle X-ray scattering patterns of SBA-15 modified with different Na loadings and calcined at 500 °C using a heating rate of 8 °C/min, together with pure SBA-15.

For all sodium loadings, when the heating rate shifts from 8 to 15 °C/min, it is possible to observe a marked decrease in the specific area, indicating a loss of the material ordered structure. This becomes more evident for the highest metal contents. In this sense, Na/SBA-15 (15) R15 shows the highest decrease in the structural ordering, probably as a result of the contribution of both factors: the high metal content and the high calcination heating rate. Meanwhile, solids with the highest specific surfaces were obtained with a heating rate of 8 °C/min. For these solids, the Na loading effect on the structural ordering could be inferred by Small-angle X-ray scattering (SAXS) analysis (Fig. 1).

As it is observed, pure SBA-15 shows three well resolved peaks, corresponding to the diffraction of planes (1 0 0), (1 1 0) and (2 0 0), typical of an hexagonal ordered pore arrangement [27,30]. After sodium incorporation, the periodic arrangement of SBA-15 remains. However, while the metal loading increases, the peaks intensity decreases, which indicates a relative loss of the ordered structure.

Consequently, the sodium loadings and the employed calcination ramps influence FAME yield. This fact might be easily visualized in Fig. 2.

All the catalysts were active for biodiesel production using the described reaction conditions (Section 2.4). As expected, an increase in the catalyst sodium content results in a high biodiesel yield after 5 h of reaction. However, in general, the increment in metal content from 10 to 15 wt% does not have a significant impact.

As a tendency, the FAME yield grows by increasing the heating rate, up to 8 °C/min. Then, for all the sodium loadings, a shift of the heating rate from 8 to 15 °C/min does not lead to an important improvement in the catalysts activity.

Therefore, a theoretical sodium loading of 10 wt% and a calcination heating rate of 8 °C/min seems to be the optimum synthesis conditions to reach a catalyst with good structural regularity and area values, together with a high FAME yield (about 90%).

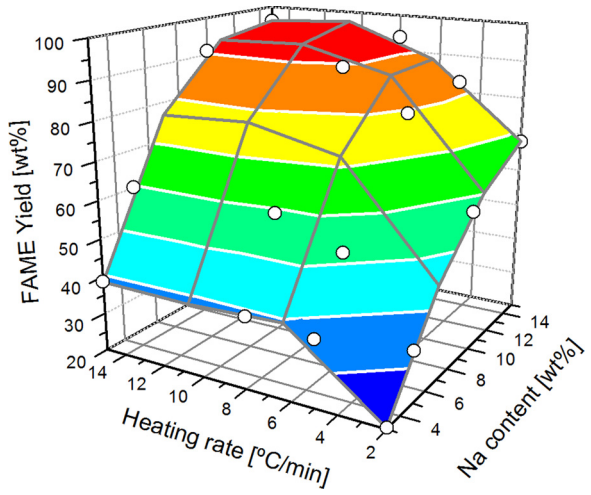


**Fig. 2.** FAME yield versus metal loading and calcination heating rate (○ Experimental data).

The results presented herein were taken as the starting point, in order to elucidate the responsible species of the catalytic activity, and the influence of the synthesis conditions on their formation.

Following this study, Fig. 3 shows the high angle XRD profiles of Na modified SBA-15 materials calcined with an 8 °C/min ramp, together with the pure SBA-15. These patterns show the amorphous silica typical peak (~22°) [34], besides characteristic peaks attributed to sodium basic and super basic species [35,36], which appear and grow for the highest loaded samples. For Na/SBA-15 (3), these peaks cannot be seen, indicating that the sodium species are amorphous or clusters too small to be detected by this technique [37]. These species may be very finely dispersed on the silica support [34].

The catalysts with large sodium contents present big sodium oxides species, as crystalline phases. Thus, when the Na loading increases, oxides species tend to agglomerate to form such ordered crystalline phases, which could provoke the marked decrease in the exposed catalytic surface (Table 1).

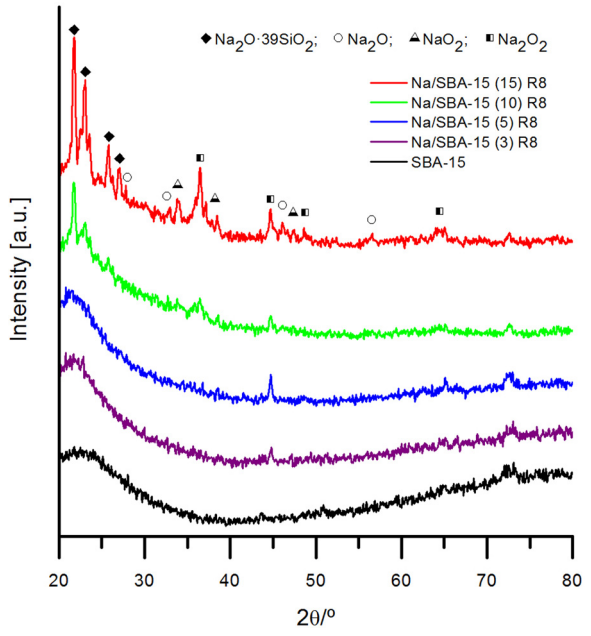


**Fig. 3.** High angle X-ray diffraction patterns of SBA-15 modified with different Na loadings and calcined at 500 °C using a heating rate of 8 °C/min, together with pure SBA-15.

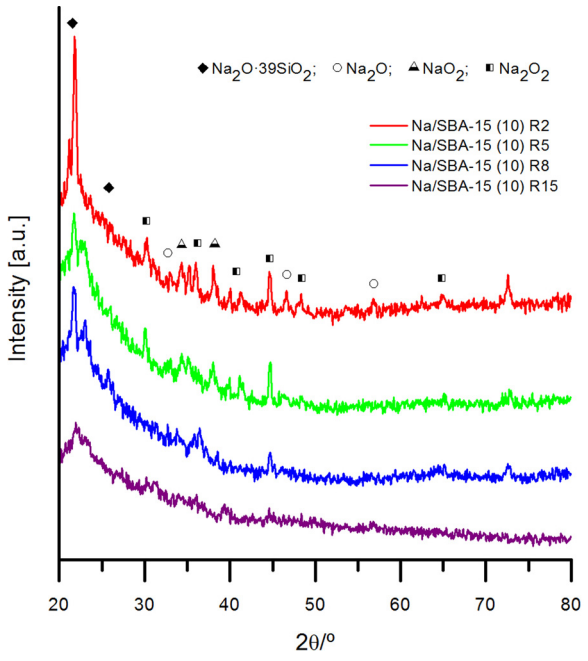


**Fig. 4.** High angle X-ray diffraction patterns of Na/SBA-15 (10) calcined at 500 °C with different heating rates.

This fact, added to that for Na/SBA-15 (15) R8 the actual metal loading is lower than the theoretical (Table 1), can explain why no significant differences in the activity are observed for Na/SBA-15 (10) R8 and Na/SBA-15 (15) R8.

Fig. 4 compares the patterns of Na/SBA-15 (10) samples calcined at different heating rates. It can be seen that the lowest heating rate profile (2 °C/min) shows more defined peaks, characteristic of crystalline phases with big particles. This is in agreement with its low specific surface (109 $m^2/g$).

As the heating rate increases up to 8 °C/min, the intensity of these peaks decreases, evidencing the dispersion of sodium species on SBA-15. Then, the highest heating rate (15 °C/min) leads to a sample with a XRD pattern where peaks corresponding to crystalline phases cannot be assigned. This may lead to thinking that the sodium species are finely dispersed. Nevertheless, its lowest area (52 $m^2/g$) compared to that of the other materials in the same series (see Table 1), clearly permits to infer a deterioration of the structural ordering of the mesoporous support.

In this manner, the heating rate seems to significantly impact the crystallinity of sodium species formed on the support surface, as well as on the mesoporous structure. According to Sun et al. [38], the presence of crystalline phases, corresponding to aggregated oxides and silicates (favored by low heating rates), results in their weak interaction with the mesoporous silica. Meanwhile, the absence of segregated crystalline phases (favored by high heating rates), gives account for a better dispersion of the metallic species and a strong interaction with the surface.

Moreover, crystalline phases impact negatively over the catalyst activity. A 57% FAME yield was obtained using Na/SBA-15 (10) R2, compared to the 90% when the calcination heating rate was 8 °C/min (Na/SBA-15 (10) R8) (Fig. 2). No relevant differences in the catalytic activity were observed employing ramps of 8 and 15 °C/min, due to the above mentioned material structural loss.

Infrared spectra were employed to characterize the surface property of materials. Fig. 5 shows the FT-IR spectra for SBA-15 and the metal loaded solids calcined with a heating rate of 8 °C/min.

At 3750 $cm^{-1}$, a band attributed to silanol stretching vibrations should appear, owing to the presence of surface OH groups with strong H-bonding interactions [39]. As mentioned by Sun et al. [38], this band may be invisible because of the influence of adsorbed water that

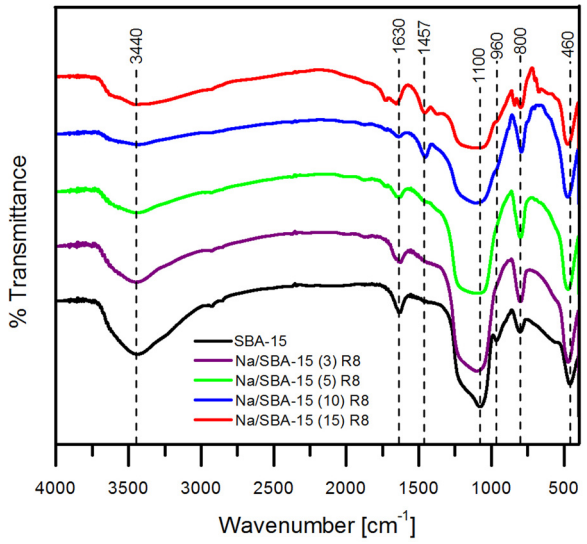


**Fig. 5.** FT-IR spectra of SBA-15 modified with different Na loadings and calcined at 500 °C using a heating rate of 8 °C/min, together with pure SBA-15.

exhibits a band at 3440 $cm^{-1}$ together with other band at 1630 $cm^{-1}$ (caused by the material hydrophilic character) [23,40,41]. However, a band at 960 $cm^{-1}$ can be attributed to Si – OH bending, which appears less defined as the Na loading increases, possibly due to the metal interaction with the support surface. The red-broadening of the band at around 1100 $cm^{-1}$, assigned to Si–O bond vibration [42,43], could also evidence this metal-silicon interaction as the sodium loading increases [14].

Bands around 800 and 460 $cm^{-1}$ correspond to Si–O–Si symmetric stretching and bending, respectively [32,44].

Finally, for the largest metal loadings, a band attributed to mono and bidentate $CO_3^{2-}$ symmetric stretching vibration appears at 1457 $cm^{-1}$ [14,21]. The presence of carbonates may be due to the interaction of the atmospheric $CO_2$ with the basic and super basic species. The intensity of $CO_3^{2-}$ band increasing with the Na loading, could indicate the gradual increase of solids basicity when the metal content increases [14,45].

On the other hand, no relevant differences in the spectra are observed when the calcination heating rate is modified for the 10 wt% Na loading sample (Fig. 6). As it can be seen, the band at 1457 $cm^{-1}$,

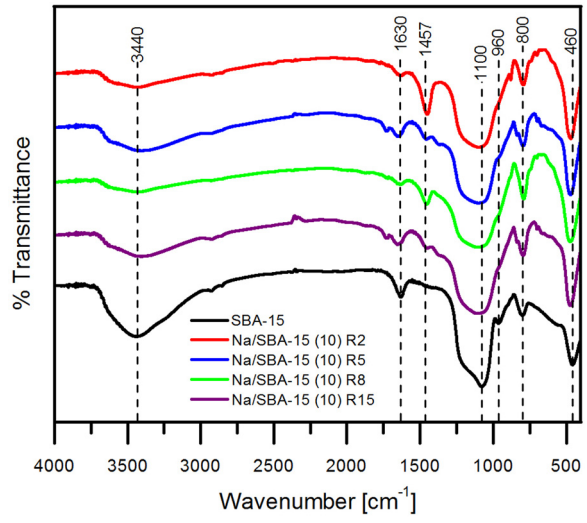


**Fig. 6.** FT-IR spectra of Na/SBA-15 (10) calcined at 500 °C with different heating rates, together with pure SBA-15.

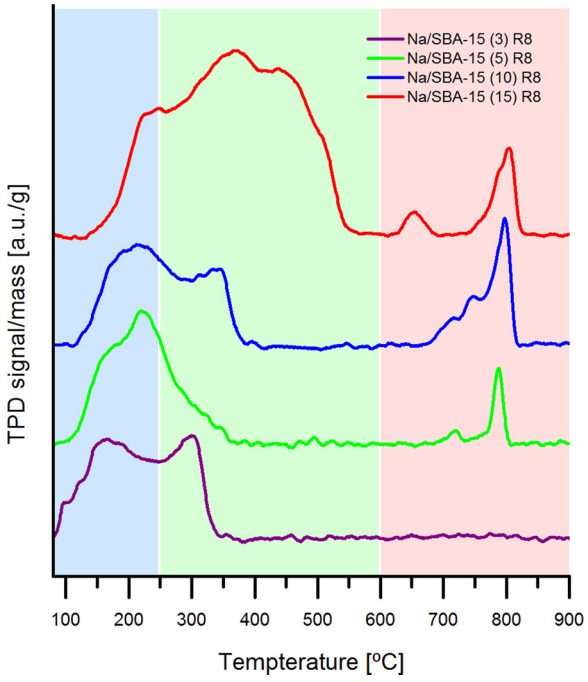


**Fig. 7.** $CO_2$ TPD profiles of SBA-15 modified with different Na loadings and calcined at 500 °C using a heating rate of 8 °C/min.

assigned to the presence of mono and bidentate carbonate, is present for all the heating rates, showing the high basicity of the materials due to Na loading [14,21]. Anyway, the band at 960 $cm^{-1}$ appears less defined with respect to the SBA-15 for all the employed heating rates, evidencing the metal-silanol interaction.

In order to evaluate the basic strength of the Na/SBA-15 synthesized materials, $CO_2$ temperature programmed desorption technique ($CO_2$ TPD) was used. Fig. 7 shows the TPD patterns of samples with different sodium loadings, calcined with a heating rate of 8 °C/min, while Table 2 summarizes the integrated areas of TPD bands.

In the graphic, three regions can be defined depending on the type of sites present in the material. The first region (up to 250 °C) corresponds to low basic strength sites. All the catalysts present a band in this region, which corresponds to the interaction of $CO_2$ with the silica [14]. The second band (250–600 °C) is attributed to the interaction with medium basic strength sites, associated to sodium silicate species ($Na_2O{\cdot}39SiO_2$) [14]. Finally, the bands appearing from 600 °C onwards evidence the presence of high basic strength sites. These sites may be attributed to sodium oxide species (considered as super base) on the catalysts surface [14,38].

Na/SBA-15(3) R8 only shows bands in the low and medium regions,

**Table 2**
Low, medium and high basic sites percentages, present in the catalysts with different sodium loadings.

| Catalyst | Low basicity sites[a] (~100–250 °C) [%] | Medium basicity sites[a] (~250–600 °C) [%] | High basicity sites[a] (~600–900 °C) [%] |
|---|---|---|---|
| Na/SBA-15 (3) R8 | 64.66 | 35.34 | – |
| Na/SBA-15 (5) R8 | 64.22 | 24.78 | 11.00 |
| Na/SBA-15 (10) R8 | 37.54 | 35.44 | 27.02 |
| Na/SBA-15 (15) R8 | 25.52 | 66.40 | 8.08 |

[a] Integrated area of TPD bands.

indicating that the material has a weak basicity.

When sodium content increases, the band corresponding to strong basic sites appears, giving account for a great catalytic activity. This basic strength can be promoted by the presence of finely dispersed sodium oxides (Lewis base sites) [4], increasing with the metal loading.

By increasing the Na loading from 5 to 10%, the band related to strong basic sites becomes more intense and its maximum is shifted to high temperatures [21], despite the fact that Na/SBA-15 (10) R8 specific surface decrease. Nevertheless, increasing the theoretical Na loading from 10% to 15% does not lead to an increment in the strong sites amount; in fact, the percentage of these sites is low (see Table 2). As it is observed, the Na/SBA-15 (15) R8 TPD profile shows a band between 400 °C and 600 °C that could be assigned to a medium basicity due to the presence of big size oxides. These crystalline phases correspond to agglomerate oxides, and have already been observed in the XRD profile of this sample. Then, the slight increase in the catalytic activity when the Na loading shifts from 10% to 15%, is probably caused by the contribution of these sites (35.44 to 66.40%, respectively).

Further, the influence of the calcination heating rate was evaluated and Fig. 8 shows the $CO_2$ TPD patterns of Na/SBA-15 (10) calcined at 2, 5, 8 and 15 °C/min. It can be seen that a high heating rate results in the appearance of desorption band at ~800 °C. This is associated to the formation of those strong basic species, which lead to an enhanced catalytic activity. However, there is an evident difference between the patterns of Na/SBA-15 (10) R8 and R15 (owing to the major presence of low and medium basic sites for the heating rate of 15 °C/min), with an apparent reduction in the strong basic sites quantity. This fact indicates that the highest heating rate is not favorable for the formation of these finely dispersed super basic oxides, and might even lead to the deterioration of the material ordered structure, as demonstrated by XRD and specific area analysis (Table 3).

On the other hand, even when the sodium loading is low (e.g. Na/SBA-15 (3)) or the heating rate is low (2 °C/min to 5 °C/min), a transesterification activity is still detected. The presence of silicate species with weak basicity showed on the TPDs patterns could be responsible for this behavior.

In order to follow the investigation on the nature of the active species over the catalysts, XPS analysis was performed and the results

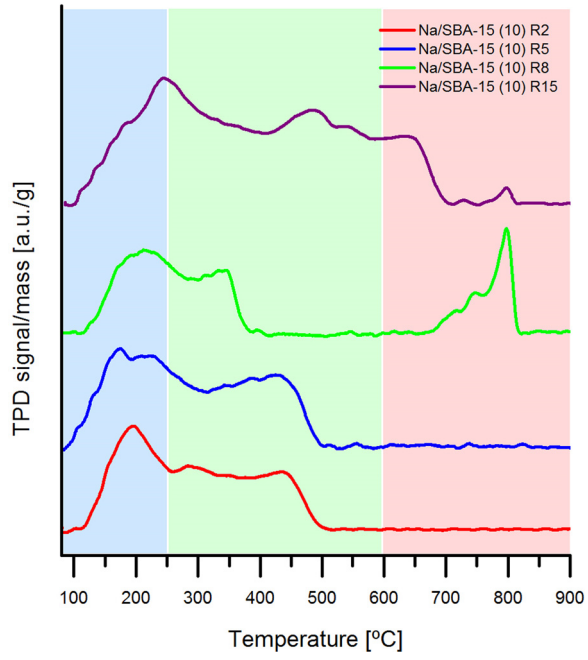


**Fig. 8.** $CO_2$ TPD profiles of Na/SBA-15 (10) calcined at 500 °C with different heating rates.

**Table 3**
Low, medium and high basic sites percentages, present in the catalysts calcined with different heating rates.

| Catalyst | Low basicity sites[a] (~100–250 °C) [%] | Medium basicity sites[a] (~250–600 °C) [%] | High basicity sites[a] (~600–900 °C) [%] |
|---|---|---|---|
| Na/SBA-15 (10) R2 | 42.10 | 57.90 | – |
| Na/SBA-15 (10) R5 | 43.19 | 56.81 | – |
| Na/SBA-15 (10) R8 | 37.54 | 35.44 | 27.02 |
| Na/SBA-15 (10) R15 | 22.68 | 65.35 | 11.96 |

[a] Integrated area of TPD bands.

**Table 4**
Binding energy of the catalyst synthetized with different sodium contents and calcined with an 8 °C/min heating rate.

| Catalyst | Si 2p [eV] | O 1s [eV] | Na 1s [eV] | C 1s[a] [eV] |
|---|---|---|---|---|
| SBA-15 | 103.5 | 533.0 | – | 284.6 |
| Na/SBA-15 (3) R8 | 102.0 | 531.3 | 1070.4 | 284.6 |
| Na/SBA-15 (5) R8 | 102.6 | 531.9 | 1071.1 | 284.6 |
| Na/SBA-15 (10) R8 | 102.7 | 532.0 | 1071.2 | 284.6 |
| Na/SBA-15 (15) R8 | 102.8 | 532.2 | 1071.2 | 284.6 |

[a] C 1 s signal was adjusted at 284.6 eV.

**Table 5**
Superficial composition of the catalysts calcined with an 8 °C/min heating rate.

| Catalyst | Si 2s [%] | Si 2p [%] | O 1s [%] | Na 1s [%] | Na AA[a] [%] |
|---|---|---|---|---|---|
| Na/SBA-15 (3) R8 | 22.19 | 26.63 | 48.92 | 2.26 | 3.2 |
| Na/SBA-15 (5) R8 | 21.76 | 26.77 | 47.49 | 3.98 | 4.4 |
| Na/SBA-15 (10) R8 | 20.46 | 25.07 | 46.28 | 8.19 | 10.3 |
| Na/SBA-15 (15) R8 | 19.57 | 23.77 | 45.44 | 11.22 | 12.4 |

[a] Sodium bulk content, measured by atomic absorption spectroscopy (AA).

are displayed in Tables 4, 5 and Fig. 9.

As expected, the signal obtained from XPS for all the samples confirms the presence of sodium oxides (Fig. 9a). Na 1s exhibits a symmetric peak, and its relative intensity grows in consistency with the metal loading increase.

It is interesting to point that O 1s signal (Fig. 9b) becomes asymmetrical as the metal loading increases, which can be assigned to the contribution of two components: one at ~529 eV corresponding to the sodium species, and another at ~532 eV, assigned to the siliceous support [21]. The contribution from the sodium oxides (that shifts the oxygen peak to lower binding energies and increases with the Na content) could occur as a result of the Si–O–Na bonds formation on the catalyst surface after impregnation and calcination. These bonds would stabilize metal oxides and silicates on the support surface [46]. This shift to low binding energies can also be detected in Si 2p signal for all the catalysts (Table 4), comparing to the support (103.5 eV), which suggest the existence of such interaction between the SBA-15 and metal species. Finally, a slight diminution in the binding energy of Na 1s signal with respect to "bulk sodium oxide" (1072.3 eV), would also indicate this interaction between the active species and the support [46].

Furthermore, in Table 5 and supplementary material S1, it can be observed that the total sodium content determined by AA is higher than the superficial Na content (detected by XPS), suggesting the incorporation of the sodium species inside SBA-15 channels.

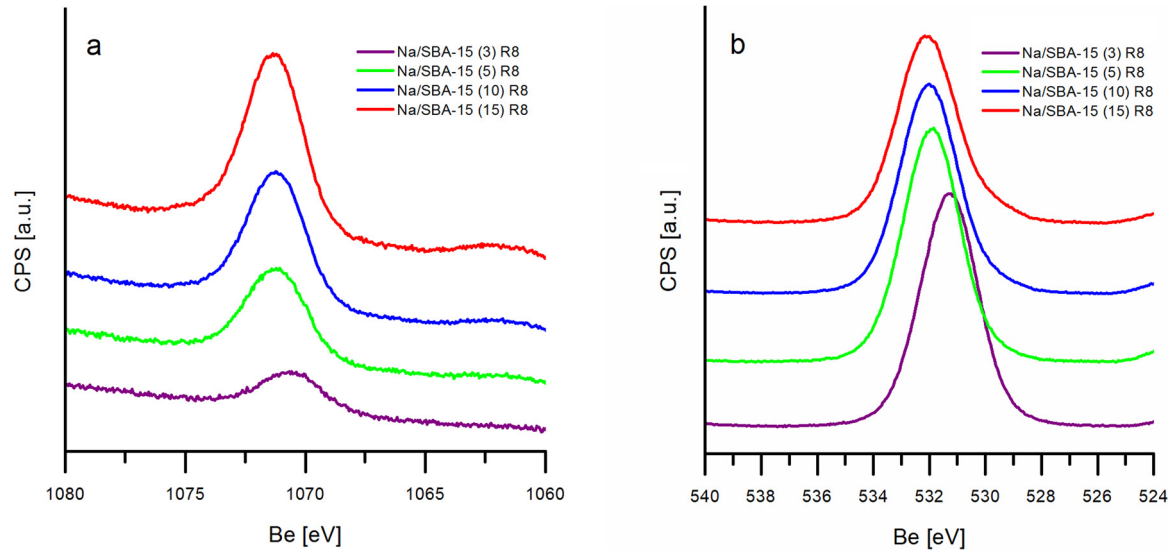


**Fig. 9.** (a) Na 1s and (b) O 1s XPS spectra.

As mentioned in the Introduction, the methoxides formed on the catalyst surface are the responsible for reacting with the triglycerides present in the liquid phase [4]. In other words, the triglyceride does not directly interact with the catalyst surface. This is why the amount and nature of active species deposited on the catalyst surface are important for the studied reaction. Thus, a 10 wt% sodium loading seems to be the optimal to achieve a high content of finely dispersed super basic Na oxides, which are the active centers for methoxide formation. A good dispersion of these species can be obtained employing a high calcination heating rate (up to 8 °C/min), according with the results exposed in this work.

It is necessary to remark that an increase in the metal loading above 10 wt% as well as a sufficiently low heating rate (2 °C/min) allow the formation of oxide crystalline phases with less basic strength, which do not significantly impact in the development of the reaction. According to Knözinger et al. [47], the formation of highly dispersed species or crystalline phases in the supported catalyst synthesis, is governed by nucleation and growth mechanisms. For this purpose, the active phase must become mobile, leading to a liquid-like behavior of the surface layer.

For the sintering of small particles deposited on a support surface, several mechanisms have been proposed [47]: migration of crystallites and their coalescence; emission of atoms from small crystallites and their capture by large ones; or a combination of both of them.

For the studied case and in consistence with the literature [47], probably when a low heating rate is used, the active phase diffusion appears to be slow, leading to the necessary time for interaction or agglomeration forces between two particles to be established. Under these conditions, the sintering phenomena (instead of migration) is favored, resulting in the formation of crystalline phases (diffusion-controlled process). Meanwhile, when the heating rate is faster enough (8 °C/min), the coalescence of two particles into one is slow compared to the diffusion time (coalescence-controlled process). As a consequence, a great dispersion of the active species on the SBA-15 is obtained, which would permit that more methanol molecules interact and form methoxides.

## 4. Conclusions

Solid base catalysts were prepared incorporating sodium in different concentrations on SBA-15, by wet impregnation method, and using different calcination heating rates. The presence of sodium oxide species on the support could be demonstrated. These solids were employed successfully in the transesterification of sunflower oil with absolute methanol. From these results, it is possible to claim that the generation of active sites for this reaction can be controlled by both studied synthesis variables: sodium content and calcination heating rate.

The use of 10 wt% sodium loading on the SBA-15 and 8 °C/min calcination heating rate were established as the optimal synthesis conditions, which allowed reaching a high concentration of active centers with strong basicity, finely dispersed on the support. Using this catalyst, a 90% FAME yield was obtained after 5 h of reaction.

## Acknowledgements

The authors are grateful to: ANCyT, CONICET-FYPF and UTN for the financial support through PICT-2015-0905, PIO 13320150100014CO and PID UTN4402. The thanks are also given to ANPCyT for the purchase of the SPECS multitechnique analysis instrument (PME8-2003). Joana Maia Dias is an integrated member of LEPABE, financed by POCI-01-0145-FEDER-006939 (Laboratório de Engenharia de Processos, Ambiente, Biotecnologia e Energia, UID/EQU/00511/2013), FEDER through COMPETE2020 - Programa Operacional Competitividade e Internacionalização (POCI) and by national funds through FCT - Fundação para a Ciência e a Tecnologia.

## Appendix A. Supplementary data

Supplementary material related to this article can be found, in the online version, at doi:https://doi.org/10.1016/j.mcat.2018.08.013.

## References

[1] G. Knothe, L.F. Razon, Biodiesel fuels, Prog. Energy Combust. Sci. 58 (2017) 36–59, https://doi.org/10.1016/j.pecs.2016.08.001.
[2] G. Pahl, S.D.S.B. McKibben, Biodiesel: Growing a New Energy Economy, 2nd edition, Chelsea Green Publishing, White River Junction, 2008 https://books.google.com.ar/books?id=gJIyU-DWYPoC.
[3] A.K. Endalew, Y. Kiros, R. Zanzi, Inorganic heterogeneous catalysts for biodiesel production from vegetable oils, Biomass Bioenergy 35 (2011) 3787–3809, https://doi.org/10.1016/j.biombioe.2011.06.011.
[4] R. Verhé, C. Echim, W. De Greyt, C. Stevens, Production of biodiesel via chemical catalytic conversion, in: R. Luque, J. Campelo, J. Clark (Eds.), Handb. Biofuels Prod. Woodhead Publishing Limited, Philadelphia, 2011, pp. 97–133, https://doi.org/10.1533/9780857090492.2.97.
[5] A. Demirbas, Importance of biodiesel as transportation fuel, Energy Policy 35 (2007) 4661–4670, https://doi.org/10.1016/j.enpol.2007.04.003.
[6] A. Casas, C.M. Fernández, M.J. Ramos, Á. Pérez, J.F. Rodríguez, Optimization of the reaction parameters for fast pseudo single-phase transesterification of sunflower oil, Fuel 89 (2010) 650–658, https://doi.org/10.1016/j.fuel.2009.08.004.

[7] J.M. Dias, M.C.M. Alvim-Ferraz, M.F. Almeida, Comparison of the performance of different homogeneous alkali catalysts during transesterification of waste and virgin oils and evaluation of biodiesel quality, Fuel 87 (2008) 3572–3578, https://doi.org/10.1016/j.fuel.2008.06.014.

[8] A.C. Dimian, C.S. Bildea, Chemical Process Design: Computer-Aided Case Studies, WILEY-VCH, Weinheim, 2008, https://doi.org/10.1002/9783527621583.

[9] B. Freedman, E.H. Pryde, T.L. Mounts, Variables affecting the yields of fatty esters from transesterified vegetable oils, J. Am. Oil Chem. Soc. 61 (1984) 1638–1643, https://doi.org/10.1007/BF02541649.

[10] M.R. Anuar, A.Z. Abdullah, Challenges in biodiesel industry with regards to feedstock, environmental, social and sustainability issues: a critical review, Renew. Sustain. Energy Rev. 58 (2016) 208–223, https://doi.org/10.1016/j.rser.2015.12.296.

[11] M. Ayoub, A.Z. Abdullah, Critical review on the current scenario and significance of crude glycerol resulting from biodiesel industry towards more sustainable renewable energy industry, Renew. Sustain. Energy Rev. 16 (2012) 2671–2686, https://doi.org/10.1016/j.rser.2012.01.054.

[12] I.M. Atadashi, M.K. Aroua, A.R. Abdul Aziz, N.M.N. Sulaiman, The effects of catalysts in biodiesel production: a review, J. Ind. Eng. Chem. 19 (2013) 14–26, https://doi.org/10.1016/j.jiec.2012.07.009.

[13] M. Hasheminejad, M. Tabatabaei, Y. Mansourpanah, M.K. Far, A. Javani, Upstream and downstream strategies to economize biodiesel production, Bioresour. Technol. 102 (2011) 461–468, https://doi.org/10.1016/j.biortech.2010.09.094.

[14] H. Sun, J. Han, Y. Ding, W. Li, J. Duan, P. Chen, H. Lou, X. Zheng, One-pot synthesized mesoporous Ca/SBA-15 solid base for transesterification of sunflower oil with methanol, Appl. Catal. A Gen. 390 (2010) 26–34, https://doi.org/10.1016/j.apcata.2010.09.030.

[15] W. Thitsartarn, T. Maneerung, S. Kawi, Highly active and durable Ca-doped Ce-SBA-15 catalyst for biodiesel production, Energy 89 (2015) 946–956, https://doi.org/10.1016/j.energy.2015.06.039.

[16] J.S. Lee, S. Saka, Biodiesel production by heterogeneous catalysts and supercritical technologies, Bioresour. Technol. 101 (2010) 7191–7200, https://doi.org/10.1016/j.biortech.2010.04.071.

[17] T.L. Chew, S. Bhatia, Catalytic processes towards the production of biofuels in a palm oil and oil palm biomass-based biorefinery, Bioresour. Technol. 99 (2008) 7911–7922, https://doi.org/10.1016/j.biortech.2008.03.009.

[18] S. Yan, C. Dimaggio, S. Mohan, M. Kim, S.O. Salley, K.Y.S. Ng, Advancements in heterogeneous catalysis for biodiesel synthesis, Top. Catal. 53 (2010) 721–736, https://doi.org/10.1007/s11244-010-9460-5.

[19] G.O. Ferrero, E.M. Sánchez Faba, G.A. Eimer, Two products one catalyst: emulsifiers and biodiesel production combining enzymology, nanostructured materials engineering and simulation models, Chem. Eng. J. 348 (2018) 960–965, https://doi.org/10.1016/j.cej.2018.05.048.

[20] G.O. Ferrero, M.F. Almeida, M.C.M. Alvim-Ferraz, J.M. Dias, Water-free process for eco-friendly purification of biodiesel obtained using a heterogeneous Ca-based catalyst, Fuel Process. Technol. 121 (2014) 114–118, https://doi.org/10.1016/j.fuproc.2014.01.020.

[21] M.C.G. Albuquerque, I. Jiménez-Urbistondo, J. Santamaría-González, J.M. Mérida-Robles, R. Moreno-Tost, E. Rodríguez-Castellón, A. Jiménez-López, D.C.S. Azevedo, C.L. Cavalcante, P. Maireles-Torres, CaO supported on mesoporous silicas as basic catalysts for transesterification reactions, Appl. Catal. A Gen. 334 (2008) 35–43, https://doi.org/10.1016/j.apcata.2007.09.028.

[22] G. Baskar, R. Aiswarya, Trends in catalytic production of biodiesel from various feedstocks, Renew. Sustain. Energy Rev. 57 (2016) 496–504, https://doi.org/10.1016/j.rser.2015.12.101.

[23] A.I. Osman, J.K. Abu-Dahrieh, A. Abdelkader, N.M. Hassan, F. Laffir, M. McLaren, D. Rooney, Silver-Modified η-Al 2 O 3 catalyst for DME production, J. Phys. Chem. C. 121 (2017) 25018–25032, https://doi.org/10.1021/acs.jpcc.7b04697.

[24] N. Rahmat, A.Z. Abdullah, A.R. Mohamed, A review: mesoporous Santa Barbara amorphous-15, types, synthesis and its applications towards biorefinery production, Am. J. Appl. Sci. 7 (2010) 1579–1586, https://doi.org/10.3844/ajassp.2010.1579.1586.

[25] S. Soltani, U. Rashid, S.I. Al-Resayes, I.A. Nehdi, Mesoporous catalysts for biodiesel production: a new approach, in: M.G. Rasul, A.K. Azad, S.C. Sharma (Eds.), Clean Energy Sustain. Dev. Academic Press, Elsevier, Queensland, 2017, pp. 487–506, https://doi.org/10.1016/B978-0-12-805423-9.00016-8.

[26] A. Corma, From microporous to mesoporous molecular sieve materials and their use in catalysis, Chem. Rev. 97 (1997) 2373–2420, https://doi.org/10.1021/cr960406n.

[27] D. Zhao, Q. Huo, J. Feng, B.F. Chmelka, G.D. Stucky, Nonionic triblock and star diblock copolymer and oligomeric sufactant syntheses of highly ordered, hydrothermally stable, mesoporous silica structures, J. Am. Chem. Soc. 120 (1998) 6024–6036, https://doi.org/10.1021/ja974025i.

[28] V.L. Zholobenko, A.Y. Khodakov, M. Impéror-Clerc, D. Durand, I. Grillo, Initial stages of SBA-15 synthesis: an overview, Adv. Colloid Interface Sci. 142 (2008) 67–74, https://doi.org/10.1016/j.cis.2008.05.003.

[29] J.A. Sullivan, L. Sherry, Different dispersions of group II catalysts over SBA-15 and MCM-41: effects on transesterification reactivity, Catal. Commun. 60 (2015) 88–91, https://doi.org/10.1016/j.catcom.2014.11.016.

[30] D. Zhao, J. Feng, Q. Huo, N. Melosh, G.H. Fredrickson, B.F. Chmelka, G.D. Stucky, Triblock copolymer syntheses of mesoporous silica with periodic 50 to 300 angstrom pores, Science 279 (1998) 548–552, https://doi.org/10.1126/science.279.5350.548 80-..

[31] M.S. Carvalho, M.A. Mendonça, D.M.M. Pinho, I.S. Resck, P.A.Z. Suarez, Chromatographic analyses of fatty acid methyl esters by HPLC-UV and GC-FID, J. Braz. Chem. Soc. 23 (2012) 763–769, https://doi.org/10.1590/S0103-50532012000400023.

[32] T.M. Albayati, A.M. Doyle, Encapsulated heterogeneous base catalysts onto SBA-15 nanoporous material as highly active catalysts in the transesterification of sunflower oil to biodiesel, J. Nanopart. Res. 17 (2015) 1–10, https://doi.org/10.1007/s11051-015-2924-6.

[33] R. Malhotra, A. Ali, Lithium-doped ceria supported SBA − 15 as mesoporous solid reusable and heterogeneous catalyst for biodiesel production via simultaneous esterification and transesterification of waste cottonseed oil, Renew. Energy 119 (2018) 32–44, https://doi.org/10.1016/j.renene.2017.12.001.

[34] J. Tantirungrotechai, P. Thananupappaisal, B. Yoosuk, N. Viriya-Empikul, K. Faungnawakij, One-pot synthesis of calcium-incorporated MCM-41 as a solid base catalyst for transesterification of palm olein, Catal. Commun. 16 (2011) 25–29, https://doi.org/10.1016/j.catcom.2011.09.002.

[35] S. Kumar, B. Kishore, N. Munichandraiah, Electrochemical studies of non-aqueous Na–O 2 cells employing Ag-RGO as the bifunctional catalyst, RSC Adv. 6 (2016) 63477–63479, https://doi.org/10.1039/C6RA13596J.

[36] J. Mao, Q. Gu, D.H. Gregory, Revisiting the hydrogen storage behavior of the Na-O-H system, Materials (Basel) 8 (2015) 2191–2203, https://doi.org/10.3390/ma8052191.

[37] N.I. Cuello, V.R. Elías, E. Winkler, G. Pozo-López, M.I. Oliva, G.A. Eimer, Magnetic behavior of iron-modified MCM-41 correlated with clustering processes from the wet impregnation method, J. Magn. Magn. Mater. 407 (2016) 299–307, https://doi.org/10.1016/j.jmmm.2016.01.004.

[38] S. Lin Bing, H.K. Jia, Y. Chun, J. Yang, N.G. Fang, Y. Wang, H.Z. Jian, G.Z. Zhi, New attempt at directly generating superbasicity on mesoporous silica SBA-15, Inorg. Chem. 47 (2008) 4199–4208, https://doi.org/10.1021/ic702223b.

[39] T.M. Albayati, A.M. Doyle, SBA-15 Supported bimetallic catalysts for enhancement isomers production during n-heptane decomposition, Int. J. Chem. React. Eng. 12 (2014) 1–10, https://doi.org/10.1515/ijcre-2013-0120.

[40] N.R.E. Radwan, Influence of La2O3and ZrO2as promoters on surface and catalytic properties of CuO/MgO system prepared by sol-gel method, Appl. Catal. A Gen. 299 (2006) 103–121, https://doi.org/10.1016/j.apcata.2005.10.008.

[41] T. Tsoncheva, L. Ivanova, C. Minchev, M. Fröba, Cobalt-modified mesoporous MgO, ZrO2, and CeO2 oxides as catalysts for methanol decomposition, J. Colloid Interface Sci. 333 (2009) 277–284, https://doi.org/10.1016/j.jcis.2008.12.070.

[42] B. Tian, X. Liu, C. Yu, F. Gao, Q. Luo, S. Xie, B. Tu, D. Zhao, Microwave assisted template removal of siliceous porous materials, Chem. Commun. (2002) 1186–1187, https://doi.org/10.1039/B202180C.

[43] Q. Jiang, Z.Y. Wu, Y.M. Wang, Y. Cao, C.F. Zhou, J.H. Zhu, Fabrication of photoluminescent ZnO/SBA-15 through directly dispersing zinc nitrate into the as-prepared mesoporous silica occluded with template, J. Mater. Chem. 16 (2006) 1536–1542, https://doi.org/10.1039/B516061H.

[44] R.W. Cranston, F.A. Inkley, 17 The Determination of Pore Structures from Nitrogen Adsorption Isotherms, Adv. Catal. 9 (1957) 143–154, https://doi.org/10.1016/S0360-0564(08)60163-7.

[45] W. Xie, H. Peng, L. Chen, Transesterification of soybean oil catalyzed by potassium loaded on alumina as a solid-base catalyst, Appl. Catal. A Gen. 300 (2006) 67–74, https://doi.org/10.1016/j.apcata.2005.10.048.

[46] W. Xie, L. Zhao, Heterogeneous CaO–MoO3–SBA-15 catalysts for biodiesel production from soybean oil, Energy Convers. Manag. 79 (2014) 34–42, https://doi.org/10.1016/j.enconman.2013.11.041.

[47] H. Knözinger, E. Taglauer, Spreading and wetting, in: G. Ertl, H. Knözinger, J. Weitkamp (Eds.), Prep. Solid Catal. Wiley-VCH Verlag GmbH, Weinheim, Germany, 2008, pp. 501–526, https://doi.org/10.1002/9783527619528.ch4h.